A First-Principles Microkinetic Model for Low-Temperature NH3 Assisted Selective Catalytic Reduction of NO over Cu-CHA

ACS Catalysis

pubs.acs.org/acscatalysis

Research Article

First-Principles Microkinetic Model for Low-Temperature NH_3-Assisted Selective Catalytic Reduction of NO over Cu-CHA

Yingxin Feng,* Xueting Wang, Ton V. W. Janssens, Peter N. R. Vennestrøm, Jonas Jansson, Magnus Skoglundh, and Henrik Grönbeck*

Cite This: *ACS Catal.* 2021, 11, 14395−14407

Read Online

ACCESS | Metrics & More | Article Recommendations | Supporting Information

ABSTRACT: A first-principles microkinetic model is developed to investigate the low-temperature ammonia-assisted selective catalytic reduction (NH_3-SCR) of NO over Cu-chabazite (Cu-CHA). The reaction proceeds over NH_3-solvated Cu sites by the formation of H_2NNO and HONO, which decompose to N_2 and H_2O over Brønsted acid sites. Nonselective N_2O formation is considered by H_2NNO decomposition over the Cu sites. The adsorption of NH_3 at oxidized Cu sites is found to inhibit the reaction at low temperatures by hindering NO adsorption. For the reactions, we find positive reaction orders with respect to NO and O_2, whereas the reaction order with respect to NH_3 is negative. The reaction orders and the obtained apparent activation energy are in good agreement with experimental data. A degree of rate control analysis shows that NH_3-SCR over a pair of $Cu(NH_3)_2^+$ is mainly controlled by NO adsorption below 200 °C, whereas the formation of HONO and H_2NNO becomes controlling at higher temperatures. The successful formulation of a first-principles microkinetic model for NH_3-SCR rationalizes previous phenomenological models and links the kinetic behavior with materials properties, which results in unprecedented insights into the function of Cu-CHA catalysts for NH_3-SCR.

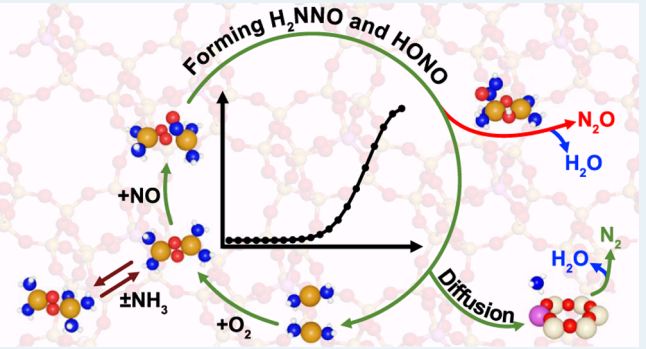

KEYWORDS: *first-principles microkinetic modeling, Cu-CHA, NH_3-SCR, N_2O formation, entropy evaluation*

INTRODUCTION

Combustion in oxygen excess is energy-efficient but requires catalytic aftertreatment systems to control NO_x emissions.[1] The current technology for lean-burn NO_x reduction is selective catalytic reduction (SCR) with ammonia as the reducing agent (NH_3-SCR), which reduces NO_x emissions efficiently.[1] Catalysts based on Cu-chabazite (Cu-CHA) are common catalysts for NH_3-SCR thanks to the low-temperature activity and good hydrothermal stability.[1−3] The overall NH_3-SCR reaction with only NO (standard SCR) is

$$4NH_3 + 4NO + O_2 \rightarrow 4N_2 + 6H_2O \quad \text{(R1)}$$

This is a redox reaction that requires catalytic sites that can change oxidation state during the reaction, which for Cu means an alternation between Cu^I and Cu^{II}. The NH_3-SCR reaction has been kinetically characterized by measurements of apparent activation energies and reaction orders. Under typical conditions for low-temperature NH_3-SCR (150−250 °C), the apparent activation energy for NH_3-SCR has been reported to be in the range of 0.4−0.8 eV.[4−6] The range in apparent activation energies can be ascribed to differences in Cu loading and presence of H_2O. The reaction order for NO conversion with respect to O_2 has been measured to be between 0.2 and 0.5,[4,7] whereas the reaction order with respect to NO is 0.7−0.9.[4,7] Furthermore, the reaction order with respect to NH_3 is zero or slightly negative when the NH_3-to-NO_x ratio is close to 1,[4] indicating that NH_3 inhibits the NH_3-SCR reaction. The reaction order of NH_3 depends on the NH_3-to-NO_x ratio and has recently been measured to be positive at low (0.1−0.5) ratios.[8]

An unwanted side reaction during NH_3-SCR is the partial reduction of NO to N_2O, which is a potent greenhouse gas receiving increasing attention.[9] One proposed overall reaction for N_2O formation is

$$2NH_3 + 2NO + O_2 \rightarrow N_2 + N_2O + 3H_2O \quad \text{(R2)}$$

Different mechanistic reaction paths may exist for N_2O formation, and NH_4NO_3 has been discussed as an intermediate at high temperatures (above 250 °C).[10−12] However, N_2O is formed also at lower temperatures over Cu-CHA and the N_2O formation profile has been measured to follow that of NH_3-

Received: August 31, 2021
Revised: October 20, 2021
Published: November 15, 2021

https://doi.org/10.1021/acscatal.1c03973
ACS Catal. 2021, 11, 14395−14407

SCR.[6,13] The apparent activation energy for low-temperature N_2O formation has been measured to be 0.36 eV,[14] which is lower than the apparent activation energy for the NH_3-SCR reaction.

In recent years, significant advances have been made in the understanding of the active sites and the reaction mechanism of low-temperature NH_3-SCR reaction over Cu-CHA catalyst. The current understanding is based on in situ X-ray absorption spectroscopy experiments in combination with density functional theory (DFT) calculations. It is now established that the ion-exchanged Cu does not occupy fixed positions in the zeolite during low-temperature operation but forms instead mobile NH_3-solvated complexes.[15−20]

The adsorption of O_2 is a key step in the reaction mechanism, which requires a pair of $[Cu(NH_3)_2]^+$ complexes, forming $[Cu_2(NH_3)_4O_2]^{2+}$ species.[17,21−24] Activation of O_2 induces the change in oxidation state of Cu from Cu^I to Cu^{II} (and possibly Cu^{III}),[25,26] which is known to be the active oxidation state for the subsequent NH_3-assisted NO reduction.[27] Two atomistic reaction cycles for low-temperature NH_3-SCR involving $[Cu(NH_3)_2]^+$ complexes and Brønsted acid sites were proposed recently based on density functional theory (DFT) calculation.[18] The activation of oxygen and the formation of the key intermediates HONO and H_2NNO were suggested to occur over the Cu sites, whereas the Brønsted acid sites facilitate the subsequent decomposition of HONO and H_2NNO to N_2 and H_2O. The two proposed cycles differ in the way NO is adsorbed on the $[Cu_2(NH_3)_4O_2]^{2+}$ complex; NO adsorbs either on the Cu cation, forming nitrosonium (NO^+), or on an O atom forming a nitrite (NO_2^-). The measured correlation between low-temperature N_2 and N_2O formation suggests a reaction path where N_2O formation is connected to the NH_3-SCR reaction cycle. We have recently presented a DFT-based mechanism for H_2NNO decomposition into N_2O and H_2O over a $[Cu_2(NH_3)_4OOH]^{2+}$ complex.[12] The proposed reaction paths for N_2 and N_2O formation have flat potential energy landscapes,[12,18] with the highest barriers related to the formation and decomposition of H_2NNO. However, these reaction mechanisms have not been evaluated by microkinetic modeling and their kinetic behaviors are presently unknown.

Phenomenological kinetic models have previously been developed for the NH_3-SCR reaction over Cu-CHA.[14,28−31] These models generally treat the SCR reaction, N_2O formation, and NH_3 oxidation as global steps and consider schematic catalytic sites. For example, the model in ref 14 includes three catalytic sites, which are all associated with a combination of Cu and Brønsted acid sites. The formation of N_2O is modeled with two reactions describing low- and high-temperature N_2O formation, respectively.[14] The phenomenological models are based on experimental data and describe accurately steady-state and transient kinetic behavior. However, because of the lumped sites and reaction steps, the models do not provide clear links between materials properties and catalytic performance.

Herein, we develop a first-principles-based microkinetic model for NH_3-SCR over Cu-CHA, which is based on an extension of the previously proposed atomistic mechanisms for N_2 and N_2O formation.[12,18] DFT calculations are used to obtain the potential energy surfaces and the reaction kinetics is treated in the mean-field approximation. The potential energy surfaces are flat, and the reaction rate depends sensitively on changes in the entropy. Thus, the evaluation of entropy changes along the reaction path is given special attention. The results from the kinetic model are in good agreement with our kinetic experiments of apparent activation energies, reaction orders, and N_2O selectivity. The development of a successful first-principles-based microkinetic model for NH_3-SCR over Cu-CHA demonstrates the capability of first-principles kinetic models, rationalizes previous phenomenological kinetic models, and forms the basis for further improvement of NH_3-SCR catalysts.

COMPUTATIONAL AND EXPERIMENTAL METHODS

First-Principles Calculation. Spin-polarized density functional theory calculations are performed with the Vienna Ab initio Simulation Package (VASP).[32−35] The valence electrons are described with a plane-wave basis set using a cutoff energy of 480 eV, and the interaction between the valence and the core electrons is described with the projector augmented wave (PAW) method.[36,37] The number of valence electrons treated in the calculations are Cu(11), Si(4), Al(3), O(6), N(5), and H(1). The *k*-point sampling is restricted to the Γ point.

The gradient-corrected Perdew−Burke−Ernzerhof (PBE)[38] functional, augmented with a Hubbard-*U* term and van der Waals corrections, is used to describe exchange−correlation effects. A Hubbard-*U* term for Cu 3d is needed to properly describe enzymatic systems[39,40] with a similar Cu−OO−Cu core structure as the oxidized Cu species present during NH_3-SCR over Cu-CHA. Here, we use a *U*-parameter of 6 eV for Cu 3d, which has been determined by comparisons with the crystal structure of Cu_2O.[39] In addition, Grimme-D3 corrections have been applied to account for the van der Waals interactions of the molecules in the zeolites.[41,42]

For the structure optimization, the convergence criterion in the self-consistent field (SCF) loop is set to 1×10^{-5} eV and the structures are considered to be relaxed when the force acting on each atom is less than 0.02 eV/Å. Transition-state structures and activation energies are calculated using the climbing image nudged elastic band (CI-NEB) method.[43,44] The transition-state structures are confirmed by vibrational analysis using the finite difference method. The search for low-energy structures is done by geometry-optimizing configurations obtained from Born−Oppenheimer ab initio molecular dynamics (AIMD) simulations, which are performed in the canonical (NVT) ensemble using a Nosé−Hoover thermostat.[45,46]

The chabazite structure is described in the rhombohedral unit cell, which contains 12 tetrahedral Si sites. The experimentally determined lattice parameters ($\alpha = \beta = \gamma = 94.2°$, $a = b = c = 9.42$ Å) are used and fixed during the structural optimizations. To model Cu-exchanged CHA, two Si atoms in the six-membered ring of the zeolite cages are replaced by Al yielding a Si/Al ratio of 5. This ratio is similar to common experimental values[6,19,47] and, thus, is a reasonable choice when modeling the Cu-CHA material for NH_3-SCR. A structural model of the cabazite cages, with a $[Cu_2(NH_3)_4O_2]^{2+}$ complex and the considered Al distribution, is shown in Figure 1. The CHA framework consists of large cages consisting of four-, six-, and eight-membered rings and small cages with four- and six-membered rings.

Microkinetic Modeling. Mean-field microkinetic modeling is used to simulate the reaction kinetics. The numerical solution of the equilibrium reaction rate and coverages are obtained by solving a set of coupled ordinary differential equations, which describe the time evolution of the adsorbate coverages. The differential equation for adsorbate *i* is given by

https://doi.org/10.1021/acscatal.1c03973
ACS Catal. 2021, 11, 14395−14407

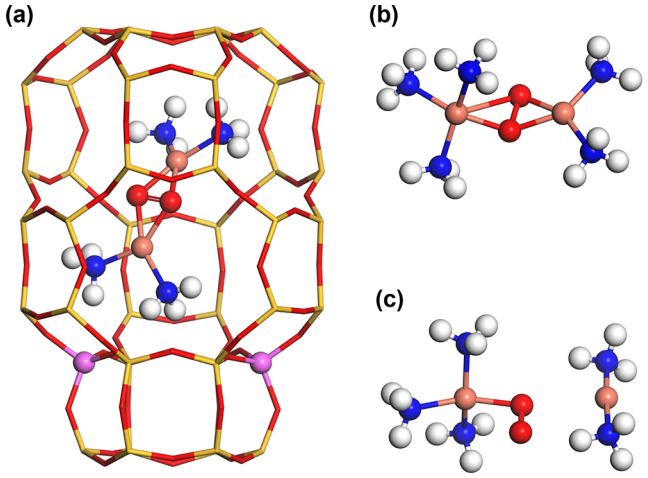

Figure 1. (a) Side view of the chabazite cages showing the Al positions in the six-membered ring. The large cage includes the $[Cu_2(NH_3)_4(O_2)]^{2+}$ complex. (b, c) Two structures of $[Cu_2(NH_3)_5(O_2)]^{2+}$. Atom color codes: Cu (bronze), Si (yellow), Al (pink), O (red), N (blue), and H (white).

$$\frac{d\theta_i}{dt} = \sum_j r_j(\vec{\theta}) c_{ji} \tag{1}$$

where θ_i is the fractional coverage of species i and r_j is the rate of reaction j, which depends on the fractional coverages ($\vec{\theta}$). The number of i molecules consumed in reaction j is reflected in the stoichiometric number (c_{ji}). The fractional coverage should in this case be understood as the fraction of Cu sites in the cycle being in a certain state. Thus, each state in the catalytic cycles represents a fractional coverage and the sum of all possible states is 1. The physical structure, composition, and action of the Cu sites change in a sequential manner along the reaction cycle, and DFT calculations show that the states are mutually exclusive. In the absence of reactants, the metal adsorption site corresponds to two $[Cu(NH_3)]_2^+$ complexes, whereas the Brønsted acid site corresponds to NH_4^+. MATLAB is used with the ode23s solver to numerically integrate the system of differential equations until steady state is reached. The mean-field approach assumes a uniform sample with random distribution of reactants and intermediates. Thus, it is applicable in cases with Cu/Al ratios where Cu- and Brønsted acid sites are spatially connected. The model assumes that Cu-complex pairs form with high enough probability. The SCR rate has experimentally shown to scale linearly[17] with Cu loadings above 0.1 Cu/1000 Å^3, and we anticipate that the model is valid for the Cu loadings in the linear regime.

The rate constants k^{TST} are computed according to the transition-state theory

$$k^{TST} = \frac{k_B T}{h} \frac{Z^{\ddagger}}{Z} \tag{2}$$

where k_B is the Boltzmann constant, T is the temperature, h is Planck's constant, Z is the partition function of the initial state, and $Z^{\ddagger}$ is the partition function of the transition state without the reaction coordinate. In the transition state theory, the initial and transition states are assumed to be in equilibrium, which leads to the following expression for the rate constant[48]

$$k^{TST} = \frac{k_B T}{h} e^{-\Delta G^{\ddagger}/k_B T} = \frac{k_B T}{h} e^{\Delta S^{\ddagger}/k_B} e^{-\Delta H^{\ddagger}/k_B T} \approx \frac{k_B T}{h} e^{\Delta S^{\ddagger}/k_B} e^{-\Delta E^{\ddagger}/k_B T} \tag{3}$$

where $\Delta G^{\ddagger}$ is the difference in Gibbs free energy between the initial and transition states, and $\Delta S^{\ddagger}$ and $\Delta H^{\ddagger}$ are the corresponding differences in entropy and enthalpy, respectively. The pV dependence on enthalpy is neglected and, hence, the change enthalpy becomes equal to the change in energy ($\Delta E^{\ddagger}$).

The reaction energy barriers for adsorption steps are zero except for O_2adsorption, which has a low activation energy. All adsorption steps are, however, associated with entropy losses, which give rise to free energy barriers indicating that the rate constants are largely determined by entropy effects.

Evaluation of Entropy Changes. Because entropy effects contribute significantly to the values for the rate constants, special care is taken when evaluating the changes in entropy. The entropies for gas-phase molecules are, as usual, calculated via their vibrational, rotational, and translational partition functions, yielding

$$S^{gas} = S^{gas}_{vib} + S^{gas}_{rot} + S^{gas}_{trans} \tag{4}$$

Here, S^{gas}_{vib}, S^{gas}_{rot}, and S^{gas}_{trans} are the vibrational, rotational, and translational entropies, respectively. It is generally challenging to describe changes in entropy during reactions in zeolites.[49,50] For NH_3-SCR in Cu-CHA, the challenge arises because some species are weakly bound and because the entropy of the adsorption site, i.e., $[Cu(NH_3)]_2^+$ complexes, is lost upon O_2 adsorption. Because of the different nature of the reactions along the reaction path, different approaches are required to describe the entropy changes.

In most cases, the harmonic approximation is used to evaluate the entropies of adsorbed species and transition states. However, in cases where the reactant enters the zeolite from the gas phase and is not chemically bound to the Cu complex, the translational and rotational entropies are estimated to be 2/3 of the gas-phase values

$$S^{zeo} = S^{zeo}_{vib} + \frac{2}{3} \times (S^{gas}_{rot} + S^{gas}_{trans}) \tag{5}$$

where S^{zeo}_{vib} is the vibrational entropy calculated in the zeolite. This approach yields reasonable values for nonbound small molecules, such as N_2 in zeolites.[18,50]

The entropy change upon O_2 adsorption forming the $[Cu_2(NH_3)_4O_2]_2^+$ complex is a special case as both O_2 and the $[Cu(NH_3)_2]^+$ complexes lose entropy during the reaction. The entropies of $[Cu(NH_3)_2]^+$, $[Cu_2(NH_3)_4O_2]^{2+}$, and the transition state for O_2 adsorption are calculated by scaling the values of the gas-phase complexes according to

$$S^{zeo} = S^{zeo}_{vib} + 0.29 \times (S^{gas}_{rot} + S^{gas}_{trans}) \tag{6}$$

Here, the scaling of the rotational and translational entropies is reduced to 0.29 compared to the case with small molecules eq 5. The decreased scaling is motivated by the larger sizes of the complexes, which hinders the rotational and translational motions, resulting in an additional reduction of the entropy. The value of 0.29 has been determined by fitting temperature-programmed desorption (TPD) profiles of NH_3 from $[Cu(NH_3)_2]^+$ in Cu-CHA (see the Supporting Information (SI)). Using the scaling of $[Cu(NH_3)_2]^+$ also for the $[Cu_2(NH_3)_4O_2]^{2+}$

https://doi.org/10.1021/acscatal.1c03973
ACS Catal. 2021, 11, 14395−14407

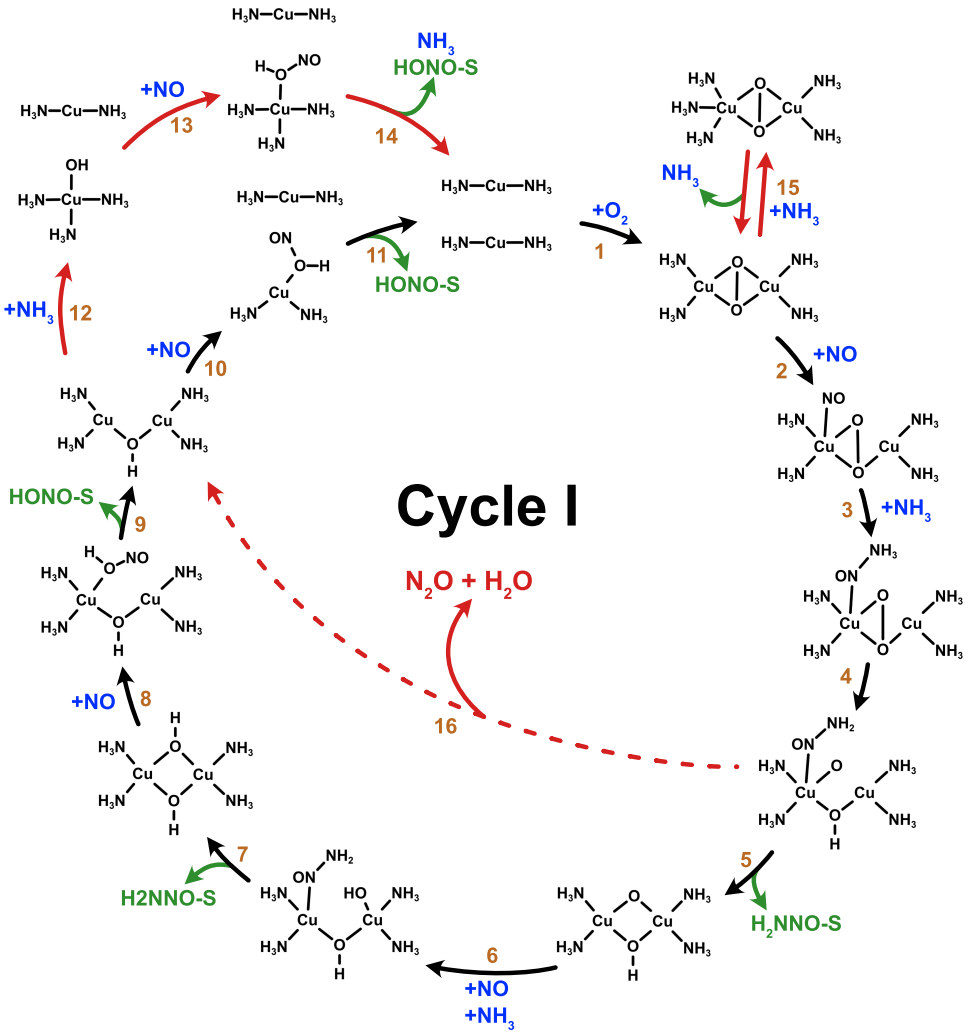

Figure 2. Proposed reaction cycle I for low-temperature NH_3-SCR over Cu-CHA.

complex, the entropy differences of O_2 adsorption in the forward reaction (ΔS_f^{zeo}) and backward reaction (ΔS_{zeo}^{b}) are evaluated as

$$\Delta S_f^{zeo} = S_{TS,[Cu_2(NH_3)_4O_2]^{2+}}^{zeo} - (2S_{[Cu(NH_3)_2]^+}^{zeo} + S_{O_2}^{gas}) \quad (7)$$

$$\Delta S_b^{zeo} = S_{TS,[Cu_2(NH_3)_4O_2]^{2+}}^{zeo} - S_{[Cu_2(NH_3)_4O_2]^{2+}}^{zeo} \quad (8)$$

where $S_{TS,[Cu_2(NH_3)_4O_2]^{2+}}^{zeo}$ and $S_{[Cu_2(NH_3)_4O_2]^{2+}}^{zeo}$ are the entropies of the transition- and final-state configurations, respectively. $S_{[Cu(NH_3)_2]^+}^{zeo}$ is the entropy of the $[Cu(NH_3)_2]^+$ complex in the zeolite. The experimentally determined value of the entropy loss for O_2 adsorption on a pair of $[Cu(NH_3)_2]^+$ complexes was recently reported to be 142 J/(mol·K),[24] which is close to our computational estimate of 152 J/(mol·K). The good agreement between computed and measured entropy changes further validates the gas-phase scaling in eq 6.

Experimental Methods. *Sample Preparation.* The Cu-CHA catalysts were prepared from the same parent H-CHA material (Si/Al ratio 6.7), via impregnation with an aqueous solution of Cu nitrate. The Cu content in the Cu-CHA catalysts was varied to 1.6 and 3.2 wt % by an adjustment of the Cu nitrate concentration in the impregnation liquid. The impregnated catalysts were dried at 100 °C and calcined in air at 500 °C for 2 h.

Kinetic Measurements. The reaction order measurements are carried out in a flow reactor with 1.6 wt % Cu-CHA. The experimental setup consists of a gas mixing system, which includes mass flow controllers (Bronkhorst Hi-Tech), a powder reactor (Setaram Sensys DSC) with a vertically mounted quartz tube (inner diameter 4 mm), and a mass spectrometer (Airsense Compact, V&F). Cu-CHA sample (11.3 mg, 1.6 wt %) (sieve fraction 300−355 μm) is placed on a sintered quartz bed in the quartz tube. The total gas flow is 300 NmL/min, and the reaction temperature is 200 °C. The sample is pretreated in O_2 at 500 °C for 30 min prior to the kinetic measurements. For the reaction order measurements with respect to NO, the concentrations of NH_3 and O_2 are held constant at 843 ppm and 10.3%, respectively. The NO concentration is varied from 88 to 722 ppm. In the measurement for the reaction order with respect to NH_3, the NO concentration and O_2 concentrations are 109 ppm and 10.3%, respectively, and the NH_3 concentration is varied between 190 and 1009 ppm. Finally, the concentration of O_2 is varied from 1.1 to 10.3% in a mixture of 381 ppm NO and 641 ppm NH_3, to measure the reaction order with respect to O_2. The reaction conditions are maintained for at least 20 min for each concentration, allowing the reaction to reach steady state. Ar is used as balance in all measurements.

https://doi.org/10.1021/acscatal.1c03973
ACS Catal. 2021, 11, 14395−14407

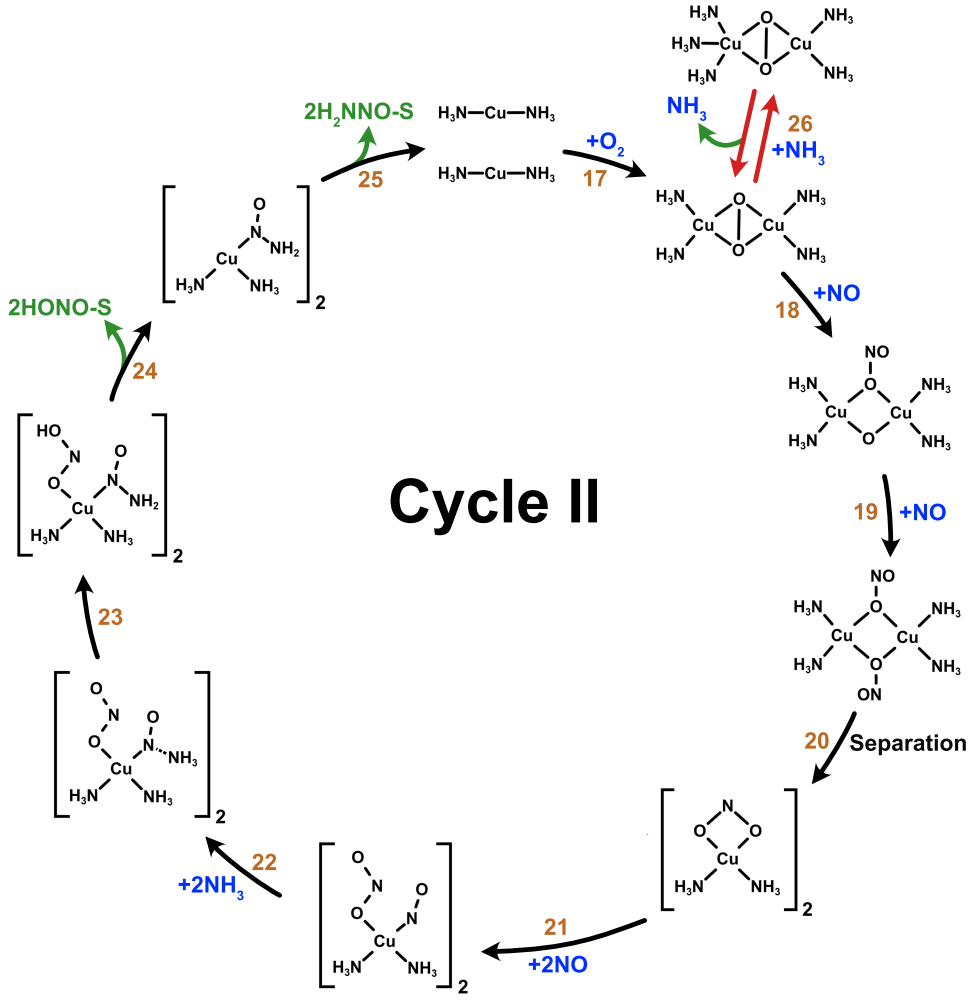

Figure 3. Proposed reaction cycle II for low-temperature NH_3-SCR over Cu-CHA.

The conversion profiles for NO_x conversion are measured in a different powder reactor setup, using 10 mg of catalyst sample in a quartz U-tube reactor (inner diameter 4 mm, sieve fraction 150−300 μm), using a feed gas consisting of 500 ppm NO, 600 ppm NH_3, 10% O_2 in N_2, at a flow rate of 300 NmL/min. A Gasmet CX4000 Fourier transform infrared (FTIR) spectrometer is used to monitor the gas composition of the reactor exit gas and the feed gas by bypassing the reactor. Prior to the measurement, the sample is heated to 550 °C, in 10% O_2 in N_2 for 30 min, after which the feed gas is admitted to the reactor. The catalyst is then cooled down stepwise to 150 °C, and for each data point, the temperature is kept constant for 30 min.

RESULTS

Catalytic Cycles and Elementary Reactions. The microkinetic models are based on the catalytic cycles for NH_3-SCR of NO to N_2 and H_2O together with N_2O formation shown in Figures 2−4. The cycles are further developments (marked by red arrows in Figures 2 and 3) of the multisite reaction mechanism suggested in ref 18. The mechanisms consist of two reaction cycles that combine the formation of HONO and H_2NNO intermediates at the Cu sites with the decomposition of these intermediates to N_2 and H_2O over Brønsted acid sites. A common step for both cycles is O_2 adsorption on a pair of $[Cu(NH_3)_2]^+$ complexes. A necessary condition to adsorb O_2 is to have two $[Cu(NH_3)_2]^+$ complexes located in the same zeolite cage. The diffusion barrier of the complexes in CHA is small,[17,51] and the probability of having two complexes in the same cage is determined by the relative stability of paired and separated complexes. Based on the literature,[17,52] we estimate the relative stability of having two complexes in the same cage to be 0.3 eV lower than having complexes in different cages. The relative stability depends on the aluminum distribution together with how far the complexes are from the original Al site and could vary by some 0.1 eV. The chosen relative stability corresponds to a probability of 6×10^{-4} having two complexes in the same cage. Assuming two complexes in the same cage, the reaction cycle starts with the O_2 adsorption step (reactions r1 and r17), when a $[Cu_2(NH_3)_4O_2]^{2+}$ complex is formed, denoted by *−OO−*, where * represents $[Cu(NH_3)_2]^+$. The adsorption of O_2 has a low energy barrier of 0.13 eV and is calculated to be exothermic by 0.20 eV. The two cycles follow different paths after the O_2 adsorption.

In cycle I (Figure 2), NO adsorbs on a Cu cation (reaction r2) forming NO−OO−*. An additional NH_3 molecule coordinates to NO−OO−* (reaction r3) and reacts (reaction r4) forming H_2NNO−OOH−*. H_2NNO desorbs from the Cu site (reaction r5) and diffuses to a Brønsted acid site (denoted by S). The reaction proceeds by subsequent NO and NH_3 adsorption and the formation of H_2NNO−OH−OH. The second H_2NNO desorbs from the Cu site and diffuses to the Brønsted acid site (reaction r7), which allows adsorption of the third NO in the

https://doi.org/10.1021/acscatal.1c03973
ACS Catal. 2021, 11, 14395−14407

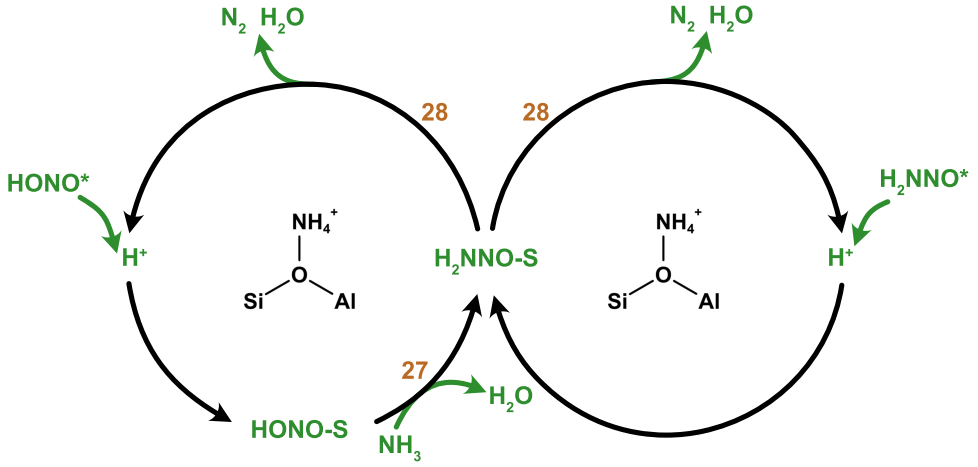

Figure 4. Proposed reaction path for HONO and H_2NNO decomposition over Brønsted acid sites.

reaction cycle (reaction r8) forming HONO−OH−*. HONO desorbs (reaction r9) and reacts further over a Brønsted acid site. Once HONO desorbs, the remaining *−OH−* can react with NO to produce a second HONO (reactions r10 and r11). One alternative reaction path is adsorption of an additional NH_3, forming NH_3−OH−* and * (reaction r12). NO can adsorb on NH_3−OH−*, forming HONO (reaction r13), which desorbs and diffuses to a Brønsted acid site in reaction r14. In reaction r14, the additional NH_3 desorbs and the second linear $[Cu(NH_3)_2]^+$ complex is restored.

The presence of *−OO−* is crucial as it allows for NO adsorption. However, NH_3 can also adsorb on *−OO−*, which was not considered in ref 18. Possible structures for NH_3 adsorption onto *−OO−* are shown in Figure 1b,c. The adsorption energy of NH_3 is in structure (b) −0.98 eV, which is larger than the adsorption energy for NO, being −0.70 eV. An alternative structure is shown in Figure 1c, where the two Cu complexes are separated and O_2 is bound to only one Cu atom. In this case, the adsorption energy is −0.94 eV. Structures (b) and (c) are separated by a barrier of 0.33 eV. The possibility for NH_3 to adsorb on the *−OO−* complex has recently been observed experimentally with X-ray absorption spectroscopy, which was assigned to be a structure similar to (c).[22] We include (b) in the reaction cycle (reaction r15) as a lumped configuration describing both (b) and (c). After the adsorption of the additional NH_3 on *−OO−*, NO cannot adsorb on that complex, which implies that NH_3 adsorption blocks the site for further reactions.

In our recent work, we proposed a possible path for N_2O formation within cycle I.[12] N_2O may form as a side reaction by direct decomposition of H_2NNO over H_2NNO−OOH−*. Once H_2NNO−OOH−* is formed after reaction r4, it is possible for H_2NNO to transfer two H atoms to the OOH−* intermediate (reaction r16) rather than to diffuse to the Brønsted acid sites (reaction r5). The decomposition of H_2NNO into N_2O and H_2O is associated with a barrier of 0.40 eV (see Figure S3 in the Supporting Information).

Turning to cycle II (Figure 3), each O site of *−OO−* will adsorb one NO forming −ONOONO− (reactions r18 and r19). The complex separates into two ONO− (reaction r20) describing adsorbed nitrites (NO_2^-). The separated complexes react subsequently with NO (reaction r21) and NH_3 (reaction r22) forming HONO−H_2NNO (reaction r23). HONO and H_2NNO desorb (reactions r24 and r25) and decompose into N_2 and H_2O at the Brønsted acid sites. At this point, the Cu sites are restored as linear complexes *. Similar to cycle I, NH_3 may adsorb on *−OO−* (reaction r26) and hinder NO adsorption. We do not consider N_2O formation in cycle II as H_2NNO cannot decompose by hydrogen transfers in this cycle.

The H_2NNO and HONO species that are generated over the Cu complexes in cycles I and II diffuse to the Brønsted acid sites and decompose into N_2 and H_2O. The paths for HONO and H_2NNO decomposition are shown in Figure 4, where S denotes a Brønsted acid site. Because NH_3 is strongly adsorbed on the Brønsted acid sites, the decomposition of H_2NNO and HONO occurs over NH_4^+. The HONO species reacts with an additional NH_3 (reaction r27) forming H_2O and H_2NNO-S, which together with H_2NNO from the Cu site can decompose into N_2 and H_2O (reaction r28). The mechanisms of H_2NNO and HONO decomposition over Brønsted acid site have previously been discussed by us[18] and are similar to those reported by Li et al.[53]

It is important to note that the reaction cycles contain four types of NH_3, with different roles in the low-temperature NH_3-SCR reaction:

1. Ligand-NH_3: NH_3 that adsorbs on the Cu cations, forming mobile $[Cu(NH_3)_2]^+$ complexes, which enable facile formation of pairs for O_2 adsorption. The ligand-NH_3 does not participate in the low-temperature SCR reaction provided that NH_3 is in excess.
2. Inhibiting NH_3: NH_3 that adsorbs strongly on the $[Cu_2(NH_3)_4O_2]^{2+}$ species, and thereby blocks the adsorption of NO, which is required for NH_3 SCR reaction.
3. Reactant-NH_3: NH_3 that takes part in the reaction by reacting with NO.
4. NH_4^+: NH_3 that is adsorbed at the Brønsted acid sites forming NH_4^+.

This means that, in low-temperature NH_3-SCR, NH_3 acts simultaneously as reactant, spectator, and inhibitor.

Kinetics for NH_3-SCR and N_2O Formation. The atomistic reaction cycles form the basis of the microkinetic model. The elementary reactions included in the microkinetic models together with the corresponding enthalpy and entropy barriers are given in Table 1. The corresponding electronic energy landscapes are shown in Figures S1 and S2 in the Supporting Information. The enthalpies for the main SCR cycles and the N_2O formation are taken from refs 12 and 18, respectively. The

https://doi.org/10.1021/acscatal.1c03973
ACS Catal. 2021, 11, 14395−14407

Table 1. Energy ($\Delta E^{\ddagger}$) and Entropy ($\Delta S^{\ddagger}$) Contributions to the Reaction Barriers of the Considered Elementary Steps[a]

no.	elementary step	$\Delta E_f^{\ddagger}$	$\Delta E_b^{\ddagger}$	$\Delta S_f^{\ddagger}$	$\Delta S_b^{\ddagger}$
	Cu—Cycle I				
	$O_2 + 2^* \overset{r_1}{\leftrightarrow} {}^*{-}OO{-}^*$	0.13	0.33	−134.9	17.6
r1	$O_2 + 2^* \overset{r_1}{\leftrightarrow} {}^*{-}OO{-}^*$ (exp . ΔE) (r1)	0.13	0.95	−134.9	17.6
r2	$NO + {}^*{-}OO{-}^* \overset{r_2}{\leftrightarrow} NO{-}OO{-}^*$ (r2)	0.00	0.70	−109.2	0.0
r3	$NH_3 + NO{-}OO{-}^* \overset{r_3}{\leftrightarrow} NH_3NO{-}OO{-}^*$ (r3)	0.00	0.31	−65.6	0.0
r4	$NH_3NO{-}OO{-}^* \overset{r_4}{\leftrightarrow} H_2NNO{-}OOH{-}^*$ (r4)	0.05	0.54	−2.5	−44.4
r5	$H_2NNO{-}OOH{-}^* + S \overset{r_5}{\leftrightarrow} H_2NNO{-}S + {}^*{-}OHO{-}^*$ (r5)	0.30	0.60	0.0	0.0
r6	$NO + NH_3 + {}^*{-}OHO{-}^* \overset{r_6}{\leftrightarrow} H_2NNO{-}OH{-}OH$ (r6)	0.16	0.60	−3.2	38.8
r7	$H_2NNO{-}OH{-}OH + S \overset{r_7}{\leftrightarrow} H_2NNO{-}S + {}^*{-}OHOH{-}^*$ (r7)	0.30	0.60	0.0	0.0
r8	$NO + {}^*{-}OHOH{-}^* \overset{r_8}{\leftrightarrow} HONO{-}OH{-}^*$ (r8)	0.10	0.39	−120.9	0.0
r9	$HONO{-}OH{-}^* + S \overset{r_9}{\leftrightarrow} HONO{-}S + {}^*{-}OH{-}^*$ (r9)	0.30	0.60	0.0	0.0
r10	$NO + {}^*{-}OH{-}^* \overset{r_{10}}{\leftrightarrow} [HONO{-}^* + {}^*]$ (r10)	0.10	1.03	−120.9	0.0
r11	$[HONO{-}^* + {}^*] + S \overset{r_{11}}{\leftrightarrow} HONO{-}S + 2^*$ (r11)	0.30	0.60	0.0	0.0
r12	$NH_3 + {}^*{-}OH{-}^* \overset{r_{12}}{\leftrightarrow} [NH_3{-}OH{-}^* + {}^*]$ (r12)	0.00	0.97	−90.4	0.0
r13	$NO + [NH_3{-}OH{-}^* + {}^*] \overset{r_{13}}{\leftrightarrow} [HONO{-}NH_3{-}^* + {}^*]$ (r13)	0.00	0.32	−120.9	0.0
r14	$[HONO{-}NH_3{-}^* + {}^*] + S \overset{r_{14}}{\leftrightarrow} NH_3 + HONO{-}S + 2^*$ (r14)	0.30	0.60	90.4	0.0
r15	$NH_3 + {}^*{-}OO{-}^* \overset{r_{15}}{\leftrightarrow} NH_3{-}OO{-}^*$ (r15)	0.00	0.98	−103.8	0.0
r16	$H_2NNO{-}OOH{-}^* \overset{r_{16}}{\leftrightarrow} N_2O + H_2O + {}^*{-}OH{-}^*$ (r16)	0.40	2.61	2.7	−301.4
	Cu—Cycle II				
r17	$O_2 + 2^* \overset{r_{17}}{\leftrightarrow} {}^*{-}OO{-}^*$ (exp . ΔE) (r17)	0.13	0.95	−134.9	17.6
r18	$NO + {}^*{-}OO{-}^* \overset{r_{18}}{\leftrightarrow} {-}ONOO{-}^*$ (r18)	0.00	1.65	−143.4	0.0
r19	$NO + {-}ONOO{-}^* \overset{r_{19}}{\leftrightarrow} {-}ONOONO{-}$ (r19)	0.00	1.65	−143.4	0.0
r20	${-}ONOONO{-} \overset{r_{20}}{\leftrightarrow} 2ONO{-}$ (r20)	0.37	0.40	−41.5	−7.4
r21	$NO + ONO{-} \overset{r_{21}}{\leftrightarrow} ONO{-}NO$ (r21)	0.00	0.91	−132.3	0.0
r22	$NH_3 + ONO{-}NO \overset{r_{22}}{\leftrightarrow} ONO{-}NONH_3$ (r22)	0.00	0.67	−65.6	0.0
r23	$ONO{-}NONH_3 \overset{r_{23}}{\leftrightarrow} HONO{-}H_2NNO$ (r23)	0.62	0.80	−14.6	12.5
r24	$HONO{-}H_2NNO + S \overset{r_{24}}{\leftrightarrow} H_2NNO{-}^* + HONO{-}S$ (r24)	0.30	0.60	0.0	0.0
r25	$H_2NNO{-}^* + S \overset{r_{25}}{\leftrightarrow} H_2NNO{-}S + {}^*$ (r25)	0.30	0.60	0.0	0.0
r26	$NH_3 + {}^*{-}OO{-}^* \overset{r_{26}}{\leftrightarrow} NH_3{-}OO{-}^*$ (r26)	0.00	0.98	−103.8	0.0
	Brønsted Acid Site				
r27	$NH_3 + HONO{-}S \overset{r_{27}}{\leftrightarrow} H_2NNO{-}S + H_2O$ (r27)	0.38	0.93	19.7	−194.6
r28	$H_2NNO{-}S \overset{r_{28}}{\leftrightarrow} H_2O + N_2 + S$ (r28)	0.38	2.08	−70.1	−294.4

[a]Reaction r20 involves the separation of the paired linear complexes, resulting in the stoichiometric 2 on the product side. Reactions r21−r25 are in the simulations doubled to account for two parallel reactions on separated complexes. Energy is given in eV and entropy in J/(mol·K). The * and S in the elementary steps represent one $[Cu(NH_3)_2]^+$ complex and one NH_4^+, respectively.

two cycles are decoupled in the simulations. The enthalpy barriers including zero-point corrections are evaluated using DFT as discussed above with the exception of O_2 adsorption. In the kinetic simulations, the adsorption energy of O_2 has been adjusted to the recently reported experimental value of 0.82 eV.[24] The difference between the experimental and calculated values can be traced to the arbitrariness in the choice of the initial state structure for the two $[Cu(NH_3)_2]^+$ complexes[24] and the issue describing molecular oxygen with the applied exchange−correlation functional.[38] In addition, the barriers for reactions r8 and r10 are set to 0.10 eV instead of the computed zero barriers to avoid numerical instabilities.

The highest energy barriers ($\Delta E^{\ddagger}$) in cycle I for NH_3-SCR are the decomposition of HONO and H_2NNO (∼0.4 eV), which is similar to the barrier for N_2O formation. The highest barrier in cycle II is instead the formation of H_2NNO, which has a barrier of 0.62 eV. The barriers for HONO and H_2NNO diffusion (0.30 eV) are based on molecular dynamics simulations, which include both desorption from the Cu sites and passage through the eight-membered zeolite rings.

https://doi.org/10.1021/acscatal.1c03973
ACS Catal. 2021, 11, 14395−14407

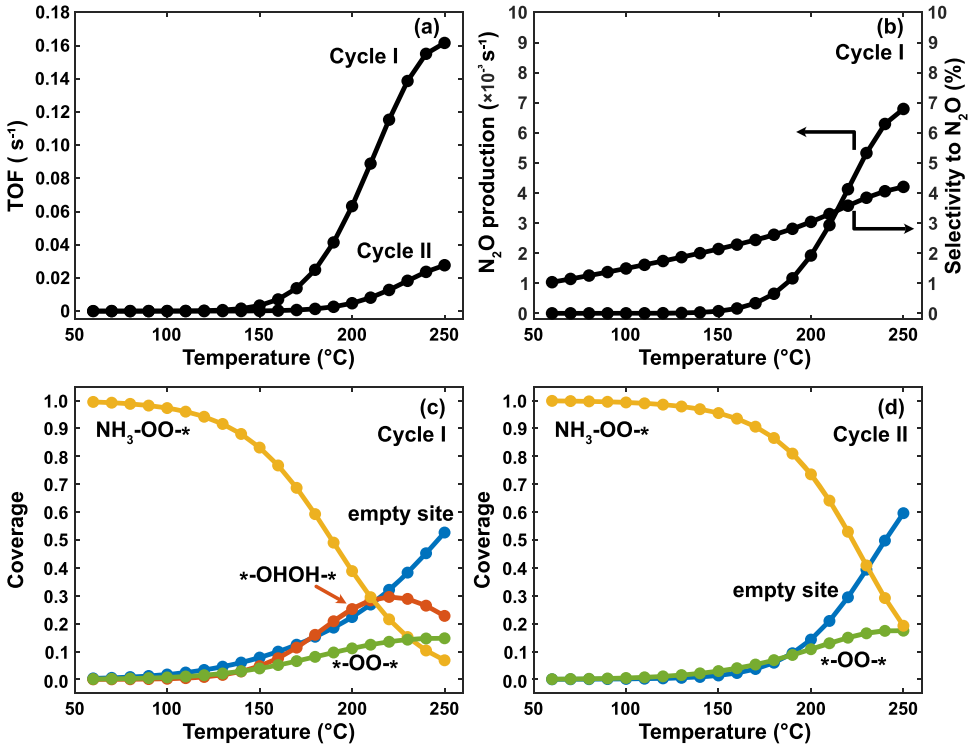

Figure 5. (a) Simulated turnover frequency for NO conversion over Cu-CHA as a function of temperature in cycles I and II. (b) N_2O formation and selectivity over Cu-CHA in cycle I. (c, d) Coverage of dominating states in cycles I and II. The fractional coverage should in this case be understood as the fraction of Cu sites being in a certain state of the reaction cycle. The simulations are performed with 600 ppm NH_3, 500 ppm NO, 10% O_2, and balance N_2.

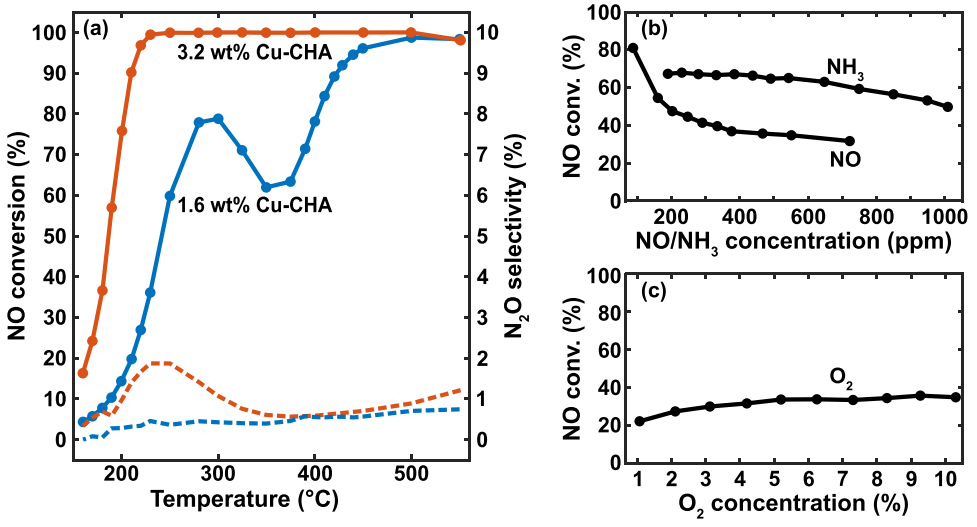

Figure 6. (a) NO conversion (solid lines) and N_2O formation (dashed lines) versus temperature for standard NH_3-SCR over the 1.6 wt % Cu-CHA (blue) and 3.2 wt % Cu-CHA (red) samples. Feed: 500 ppm NO, 600 ppm NH_3, 10% O_2, and balance N_2. The conversion at 200 °C for the 1.6 wt % Cu-CHA sample corresponds to an apparent reaction rate of 0.02 mol NO/(mol Cu·s). (b, c) NO conversion over the 1.6 wt % Cu-CHA sample versus the concentration of NO, NH_3, and O_2 at 200 °C. In this series of experiments, individual feed gas concentrations are changed when all other feed gases concentrations are held constant. NH_3 concentration is fixed to 843 ppm when the NO concentration is varied. The NO concentration is set to 139 ppm when the NH_3 concentration is varied. When the concentrations of O_2 are changed from 1 to 10%, the concentrations of NH_3 and NO are set to 641 and 381 ppm, respectively. The balancing gas in the reaction order experiments is Ar.

As we consider the reaction over $[Cu(NH_3)_2]^+$ complexes, the cycles describe standard NH_3-SCR in the low-temperature regime (below ~250 °C), where the decomposition of the $[Cu(NH_3)_2]^+$ complex is negligible.[54] The model does not describe the reaction above ~250 °C, where the contribution of framework-bound Cu becomes important.[54] The simulations are performed for a total pressure of 1 atm, with 600 ppm NH_3, 500 ppm NO, 10% of O_2, and balance N_2. In the absence of reactants, the ratio between pairs of $[Cu(NH_3)_2]^+$ complexes and the Brønsted acid sites is set to 1.

Turnover Frequency (TOF) and Coverages. The calculated turnover frequencies (TOFs) of cycles I and II are presented in

https://doi.org/10.1021/acscatal.1c03973
ACS Catal. 2021, 11, 14395−14407

Figure 5a. The TOFs in both cycles have well-defined onset temperatures of about 120 and 170 °C in cycles I and II, respectively. The TOF of cycle I is significantly higher than that of cycle II. In both cases, the TOF begins to decrease at temperatures above ∼235 °C. The decrease in TOF is due to low surface coverages as the decomposition of the $[Cu(NH_3)_2]^+$ complexes is not included in our model. The TOF is calculated as the number of consumed NO per Cu complex accounting for the probability of having two Cu complexes in the same CHA cage.

By comparing the turnover frequency and the coverages of the most abundant species reported in Figure 5c,d, it is clear that NH_3 adsorption inhibits the NH_3-SCR reaction in the low-temperature regime (<120 °C). The coverage of inhibiting NH_3 (denoted by NH_3−OO−*) is close to 1 below 100 °C for cycle I, whereas this regime extends to 150 °C for cycle II. The inhibiting NH_3 desorbs as the temperature is increased, allowing for the adsorption of NO and the formation of H_2NNO and HONO. The TOF increases with increasing *−OHOH−* coverage, which peaks at 230 °C. The number of empty sites increases and begins to dominate above 230 °C, yielding a decrease in the TOF at high temperatures. The analysis of the coverages shows that the reaction at low temperatures is determined by the adsorption energy of the NH_3 that blocks the *−OO−* sites. A weaker bond strength of NH_3−OO−* would facilitate the reaction at lower temperatures.

Figure 5b shows the TOF and the corresponding selectivity for N_2O formation in cycle I. The temperature dependence of N_2O formation is similar to that of NH_3-SCR with a peak at 230 °C. This is in agreement with experimental reports[55,56] and a consequence of N_2O formation over Cu sites via H_2NNO. The selectivity to N_2O increases from 2 to 4% in the temperature interval of 150 to 250 °C.

The NH_3-SCR reaction is a multisite reaction requiring both Cu and Brønsted acid sites, whereas N_2O formation only requires the Cu sites. This difference means that the NH_3-SCR reaction depends on both the Cu loading and the Cu/Al ratio, whereas N_2O formation depends primarily on the Cu loading. This implies that the selectivity for N_2 formation can be increased by decreasing the Cu/Al ratio. In this case, reaction r5 is favored over reaction r16 as the ratio of Brønsted acid sites is increased with respect to Cu sites.

Comparison to Experimental Data. To verify the microkinetic model, we compare the results with a set of kinetic experiments. Figure 6a shows the temperature dependence of NO conversion and N_2O selectivity for the 1.6 wt % Cu-CHA and 3.2 wt % Cu-CHA samples under standard SCR conditions. The conversion profile for the 1.6 wt % Cu-CHA catalyst shows the characteristic bimodal shape with a local maximum at about 275 °C. The onset temperature for the conversion of NO decreases with increasing Cu loading. The apparent activation energies (Table 2) derived from the NO_x conversion experiments in the 160−240 °C range are 0.62 and 0.89 eV for the 1.6 wt % Cu-CHA and 3.2 wt % Cu-CHA catalysts, respectively. The calculated apparent activation energies from the first-principles microkinetic model are 0.75 eV for cycle I including NH_3 inhibition, 0.31 eV without NH_3 inhibition (reaction r15), and 1.06 eV for cycle II with inhibition. The higher activity together with an apparent activation energy matching the experiments points to cycle I as the main reaction path for NH_3-SCR. Furthermore, the results show that the apparent activation energy for NH_3-SCR mainly is determined by the NH_3 inhibition of the $[Cu_2(NH_3)_4O_2]^{2+}$ complex. The preference of cycle I is supported by the thermodynamic preference for reaction r2 compared to reaction r18. The probability of following cycle I is about 98 % in the considered temperature regime.

Table 2. Apparent Activation Energy (E_{app}) and Reaction Orders (n_x) from Experiments and the Kinetic Models[a]

	exp.	cycle I	cycle I (without reaction r15)	cycle II	cycle II (without reaction r26)
E_{app}	0.62/0.89	0.75	0.31	1.06	0.05
n_{NH_3}	−0.23	−0.22	0.05	−0.76	0.00
n_{NO}	0.73	0.95	0.92	1.00	0.99
n_{O_2}	0.25	0.23	0.34	0.15	0.58

[a]The simulated reaction orders are evaluated at 200 °C. The energy is given in electronvolt.

The selectivity for N_2O is calculated for cycle I. To explore the dependence of the selectivity on the Cu/Al ratio, we model the formation of N_2O with different Cu/Al ratios by changing the ratio between $[Cu(NH_3)_2]^+$ and Brønsted acid sites in the model. Reducing the Cu/Al ratio to 0.33 decreases the selectivity to N_2O by a factor of 2 (see Figure S6 in the Supporting Information). The simulations match the experimental observation that N_2O formation for the 3.2 wt % Cu-CHA catalyst (Cu/Al ratio of 0.24) is significantly higher than that for the 1.6 wt % Cu-CHA catalyst (Cu/Al ratio of 0.12).

The microkinetic model also predicts reaction orders with respect to NH_3, NO, and O_2 in good agreement with experiments. Figure 6b,c shows the measured dependence of the NO_x conversion with changes in the partial pressures of NH_3, NO, and O_2 for the 1.6 wt % Cu-CHA catalyst. The reaction orders for NH_3-SCR derived from these data are −0.23 for NH_3, 0.73 for NO, and 0.25 for O_2, which are in accordance with previous measurements.[4,7,19,57] The values for NO and O_2 agree very well with the calculated values of cycle I that includes the NH_3 inhibition (−0.22 for NH_3, and 0.23 for O_2), whereas the calculated reaction order for NO (0.95) is slightly higher than the measured value. The reaction order in O_2 has been measured to decrease with increasing O_2 pressure and increasing Cu/Al ratio.[57] The model reproduces these trends as shown in the Supporting Information (Table S1). The model also predicts the experimental increase in TOF as a function of O_2 pressure (Figure S7). The reaction orders for cycle II are not in such good agreement with experiments, again indicating that cycle I is the main reaction path for NH_3-SCR.

The reaction orders analysis further exemplifies that NH_3 inhibition plays an important role in the kinetics of the NH_3-SCR reaction. The negative reaction order with respect to NH_3 is a direct consequence of the NH_3 inhibition as clearly shown by the calculated reaction order of +0.05 when omitting the NH_3 inhibition. Furthermore, the calculated apparent activation energy for cycle I becomes much lower, when the NH_3 inhibition is omitted, showing that the apparent activation energy is determined by the desorption of inhibiting NH_3. This indicates that the NH_3 inhibition is a crucial reaction that should be included in kinetic models for NH_3-SCR over Cu-CHA at low temperatures.

The discrepancy between the calculated and measured reaction order with respect to NO is probably due to effects of residual water and parallel reactions on minority Cu sites, such as framework-bound Cu, which could affect the reaction order.

https://doi.org/10.1021/acscatal.1c03973
ACS Catal. 2021, 11, 14395−14407

Degree of Rate Control Analysis for NH_3-SCR. The comparison to experiments shows that the first-principles microkinetic model captures the measured kinetic behavior. It motivates a further elaboration of which elementary steps that control the reaction by performing a degree of rate control (χ_i) analysis.[58] This analysis is performed by increasing the value of rate constants for the forward and backward reactions for each elementary step by 1% while keeping the equilibrium constant and the rate constants of all other reaction steps fixed. By calculating the response in the total TOF, the role of each elementary reaction is monitored. χ_i is calculated according to

$$\chi_i = \frac{k_i}{r}\left(\frac{\partial \mathrm{TOF}}{\partial k_i}\right)_{K_i} \tag{9}$$

The result of the degree of rate control analysis for NH_3-SCR in cycle I is shown in Figure 7. We focus on cycle I, as this cycle

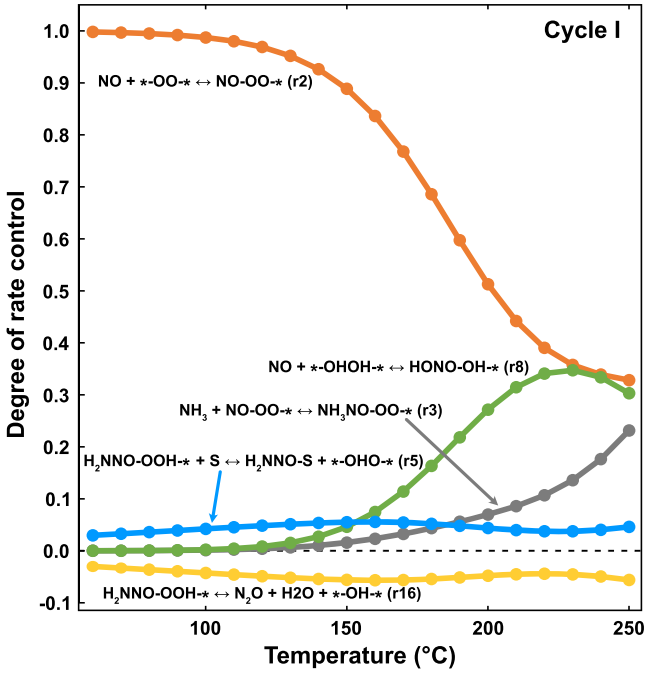

Figure 7. Degree of rate control analysis for NH_3-SCR over Cu-CHA in cycle I. The simulation is performed with 600 ppm NH_3, 500 ppm NO, 10% O_2, and balance N_2.

dominates the TOF and reproduces the measured reaction orders and apparent activation energy. Only the reactions with a notable degree of rate control are shown in Figure 7. The sum of all degrees of rate control is 1.

At low temperatures, the rate of NH_3-SCR is mainly determined by the NO adsorption step (reaction r2), as a consequence of the strong inhibition effect of NH_3. As the temperature increases to 230 °C, the controlling effect of NO adsorption is gradually reduced, whereas the formation of HONO−OH−* (reaction r8) becomes increasingly important. NO adsorption and HONO−OH−* formation reach an equal degree of rate control at 230 °C, which is the temperature for the maximum TOF. The analysis shows that the N_2O formation (reaction r16) is a competing reaction with a negative degree of rate control. The diffusion of H_2NNO (reaction r5) from the Cu site to the Brønsted acid site has an opposite degree of rate control compared to reaction r16, which signals the branching in the reaction cycle.

DISCUSSION AND SIMPLIFIED MODEL

Having access to a first-principles microkinetic model makes it possible to link the kinetic behavior to certain reaction intermediates and structures in the Cu-CHA catalyst. The apparent activation energy is related to the desorption of the inhibiting NH_3, which blocks the $[Cu_2(NH_3)_4O_2]^{2+}$ sites for NO adsorption. This explains the sizable apparent activation energy despite the flat potential energy landscape. The NH_3 inhibition is also reflected in the negative reaction order with respect to NH_3. The positive reaction order with respect to O_2 is a consequence of that O_2 adsorption is required for the NH_3-SCR reaction over $[Cu(NH_3)_2]^+$ pairs. The adsorption of O_2 changes the oxidation state from Cu^I to Cu^{II}, which allows for NO and NH_3 adsorption and the subsequent formation of H_2NNO and HONO.

The alternation between Cu^I and Cu^{II} (and possibly Cu^{III}) is central for the function of the Cu-CHA catalyst, and the temperature dependence of the Cu-oxidation state has been measured to characterize the catalyst during reaction conditions.[19,56] From an analysis of the Cu species present during the NH_3-SCR reaction, we find that the fractions of Cu^I and Cu^{II} are around 50% in the considered temperature range (150−250 °C). The fraction of Cu^{II} reaches a maximum of 57% at 210 °C and decreases to 42% at 250 °C (see Figure S9 in the Supporting Information). The calculated values match experimental reports on the basis of in situ X-ray absorption measurements.[19]

Although the microkinetic model gives a precise description of the NH_3-SCR reaction, it is a complicated reaction network that contains 18 elementary steps. To connect to previous phenomenological models, we simplify the atomistic model to only five reactions where we describe the adsorption of O_2 over a pair of $[Cu(NH_3)_2]^+$, the adsorption of NO and NH_3 on the $[Cu_2(NH_3)_4O_2]^{2+}$ complex as elementary steps and the formation of N_2 and H_2O are lumped in two steps as follows

$$O_2 + 2* \overset{R3}{\leftrightarrow} *-OO-* \tag{R3}$$

$$NO + *-OO-* \overset{R4}{\leftrightarrow} NO-OO-* \tag{R4}$$

$$NH_3 + *-OO-* \overset{R5}{\leftrightarrow} NH_3-OO-* \tag{R5}$$

$$4NH_3 + 3NO-OO-* \overset{R6}{\leftrightarrow} 4N_2 + 6H_2O + 6* \tag{R6}$$

$$2NH_3 + NO + NO-OO-* \overset{R7}{\leftrightarrow} N_2 + N_2O + 3H_2O + 2* \tag{R7}$$

These reactions for low-temperature NH_3-SCR and N_2O formation (see the SI for parameters) describe the temperature dependence of the TOF with reasonable accuracy, having an apparent activation energy of 0.86 eV and reaction orders with respect to O_2, NO, and NH_3 of 0.2, 1.2, and −0.3, respectively. We find it important to treat the adsorption of O_2, NO, and NH_3 explicitly to obtain a qualitative agreement with the detailed model, which is consistent with the kinetic analysis showing that these adsorption steps control the reaction. Our simplified model can be compared to the phenomenological model in ref 14, where the lumped NH_3-SCR reaction was reported to have an apparent activation energy of 0.71 eV. Our analysis shows

https://doi.org/10.1021/acscatal.1c03973
ACS Catal. 2021, 11, 14395−14407

that the apparent activation energy is related to the desorption of NH_3 from the $[Cu_2(NH_3)_4O_2]^{2+}$ complex.

CONCLUSIONS

We have developed a first-principles microkinetic model for low-temperature NH_3-SCR and N_2O formation over Cu-CHA catalysts, based on DFT calculations and detailed entropy analysis. The model includes H_2NNO and HONO formation over mobile Cu species together with N_2 and H_2O formation over Brønsted acid sites. N_2O formation is included via H_2NNO decomposition over Cu sites. The calculated values for activation energy and reaction orders for NO, NH_3, and O_2, based on this microkinetic model, agree well with experimentally determined values. The favorable comparison between the model and the kinetic experiments strengthens the validity of the suggested multisite reaction mechanisms for low-temperature NH_3-SCR and N_2O formation over Cu-CHA.

The atomistic description allows for a clear link between kinetic behavior and materials properties. At low temperatures, NH_3 inhibits the reaction by occupying Cu sites for NO adsorption. The NH_3 inhibition is reduced with increasing temperature allowing for NO adsorption and subsequent formation of HONO and H_2NNO. The potential energy surface is flat, and the low-temperature apparent activation energy is determined by the adsorption energy of the inhibiting NH_3, which hinders the reaction at low temperatures.

We find that N_2O selectivity is moderately affected by the temperature. Thus, N_2O selectivity cannot be steered by controlling the operational temperature. However, as low-temperature N_2 formation requires both Cu and Brønsted acid sites, whereas N_2O formation requires only Cu sites, Cu/Al ratio and Al distribution may provide handles to reduce N_2O emissions.

Our work demonstrates the capabilities of first-principles microkinetic models for reactions in zeolites with dynamic active sites. The developed model advances the conceptual understanding of low-temperature NH_3-SCR over Cu-CHA, rationalizes previous phenomenological models, and can be used to further enhance the performance of the catalyst.

ASSOCIATED CONTENT

Supporting Information

The Supporting Information is available free of charge at https://pubs.acs.org/doi/10.1021/acscatal.1c03973.

Energy landscapes for cycles I and II, H_2NNO adsorption on the $[Cu(NH_3)_4OOH]^{2+}$ complex, energy profile for H_2NNO diffusion, fit of entropy scaling factor by comparison with the NH_3 temperature-programmed desorption (TPD) profiles, analysis of the effect of Cu/Al ratio on selectivity, dependence of O_2 reaction order on oxygen pressure, temperature-dependent fractions of Cu^I and Cu^{II}, parameters and results of the simplified kinetic model (PDF)

Atomic structure files (ZIP)

AUTHOR INFORMATION

Corresponding Authors

Yingxin Feng − *Department of Physics and Competence Centre for Catalysis, Chalmers University of Technology, SE-412 96 Göteborg, Sweden;* orcid.org/0000-0002-5817-4391; Email: yingxin@chalmers.se

Henrik Grönbeck − *Department of Physics and Competence Centre for Catalysis, Chalmers University of Technology, SE-412 96 Göteborg, Sweden;* orcid.org/0000-0002-8709-2889; Email: ghj@chalmers.se

Authors

Xueting Wang − *Department of Physics and Competence Centre for Catalysis, Chalmers University of Technology, SE-412 96 Göteborg, Sweden*

Ton V. W. Janssens − *Umicore Denmark ApS, DK-2970 Hørsholm, Denmark;* orcid.org/0000-0002-1225-0942

Peter N. R. Vennestrøm − *Umicore Denmark ApS, DK-2970 Hørsholm, Denmark;* orcid.org/0000-0002-6744-5640

Jonas Jansson − *Volvo Group Trucks Technology, SE-405 08 Göteborg, Sweden*

Magnus Skoglundh − *Department of Physics and Competence Centre for Catalysis, Chalmers University of Technology, SE-412 96 Göteborg, Sweden;* orcid.org/0000-0001-7946-7137

Complete contact information is available at: https://pubs.acs.org/10.1021/acscatal.1c03973

Notes

The authors declare no competing financial interest.

ACKNOWLEDGMENTS

The authors thank Lin Chen for discussions on the reaction cycles. They acknowledge financial support from the Swedish Energy Agency (47110-1). The Competence Centre for Catalysis is hosted by Chalmers University of Technology and financially supported by the Swedish Energy Agency and the member companies AB Volvo, ECAPS AB, Johnson Matthey AB, Preem AB, Scania CV AB, and Umicore Denmark ApS. The calculations have been performed at C3SE (Göteborg) through an SNIC grant.

REFERENCES

(1) Nova, I.; Tronconi, E. *Urea-SCR Technology for DeNO$_x$ after Treatment of Diesel Exhausts*; Springer Science + Business Media: New York, 2014; pp 1−10.

(2) Schmieg, S. J.; Oh, S. H.; Kim, C. H.; Brown, D. B.; Lee, J. H.; Peden, C. H.; Kim, D. H. Thermal Durability of Cu-CHA NH_3-SCR Catalysts for Diesel NO_x Reduction. *Catal. Today* **2012**, *184*, 252−261.

(3) Xin, Y.; Li, Q.; Zhang, Z. Zeolitic Materials for DeNO$_x$ Selective Catalytic Reduction. *ChemCatChem* **2018**, *10*, 29−41.

(4) Bates, S. A.; Verma, A. A.; Paolucci, C.; Parekh, A. A.; Anggara, T.; Yezerets, A.; Schneider, W. F.; Miller, J. T.; Delgass, W. N.; Ribeiro, F. H. Identification of the Active Cu Site in Standard Selective Catalytic Reduction with Ammonia on Cu-SSZ-13. *J. Catal.* **2014**, *312*, 87−97.

(5) Gao, F.; Mei, D.; Wang, Y.; Szanyi, J.; Peden, C. H. Selective Catalytic Reduction over Cu/SSZ-13: Linking Homo- and Heterogeneous Catalysis. *J. Am. Chem. Soc.* **2017**, *139*, 4935−4942.

(6) Gao, F.; Walter, E. D.; Kollar, M.; Wang, Y.; Szanyi, J.; Peden, C. H. Understanding Ammonia Selective Catalytic Reduction Kinetics over Cu/SSZ-13 from Motion of the Cu Ions. *J. Catal.* **2014**, *319*, 1−14.

(7) Shih, A. Synthesis and Characterization of Copper-Exchanged Zeolite Catalysts and Kinetic Studies on NO_x Selective Catalytic Reduction with Ammonia. Ph.D. thesis, Purdue University, 2019.

(8) Daya, R.; Keturakis, C. J.; Trandal, D.; Kumar, A.; Joshi, S. Y.; Yezerets, A. Alternate Pathway for Standard SCR on Cu-Zeolites with Gas-Phase Ammonia. *React. Chem. Eng.* **2021**, *6*, 1042−1052.

(9) Kumar, A.; Kamasamudram, K.; Currier, N.; Yezerets, A. *SCR Architectures for Low N_2O Emissions*, SAE Technical Paper Series, 2015; pp 2−7.

(10) Shan, Y.; Shi, X.; He, G.; Liu, K.; Yan, Z.; Yu, Y.; He, H. Effects of NO_2 Addition on the NH_3-SCR over Small-Pore Cu-SSZ-13 Zeolites with Varying Cu Loadings. *J. Phys. Chem. C* **2018**, *122*, 25948−25953.
(11) Cui, Y.; Gao, F. Cu Loading Dependence of Fast NH_3-SCR on Cu/SSZ-13. *Emiss. Control Sci. Technol.* **2019**, *5*, 124−132.
(12) Feng, Y.; Janssens, T. V. W.; Vennestrøm, P. N. R.; Jansson, J.; Skoglundh, M.; Grönbeck, H. The Role of H^+- and Cu^+-Sites for N_2O Formation during NH_3-SCR over Cu-CHA. *J. Phys. Chem. C* **2021**, *125*, 4595−4601.
(13) Clark, A. H.; Nuguid, R. J. G.; Steiger, P.; Marberger, A.; Petrov, A. W.; Ferri, D.; Nachtegaal, M.; Kröcher, O. Selective Catalytic Reduction of NO with NH_3 on Cu-SSZ-13: Deciphering the Low and High-Temperature Rate-Limiting Steps by Transient XAS Experiments. *ChemCatChem* **2020**, *12*, 1429−1435.
(14) Olsson, L.; Wijayanti, K.; Leistner, K.; Kumar, A.; Joshi, S. Y.; Kamasamudram, K.; Currier, N. W.; Yezerets, A. A Multi-Site Kinetic Model for NH_3-SCR over Cu/SSZ-13. *Appl. Catal., B* **2015**, *174*−*175*, 212−224.
(15) Shwan, S.; Skoglundh, M.; Lundegaard, L. F.; Tiruvalam, R. R.; Janssens, T. V. W.; Carlsson, A.; Vennestrøm, P. N. Solid-State Ion-Exchange of Copper into Zeolites Facilitated by Ammonia at Low Temperature. *ACS Catal.* **2015**, *5*, 16−19.
(16) Negri, C.; Borfecchia, E.; Cutini, M.; Lomachenko, K. A.; Janssens, T. V. W.; Berlier, G.; Bordiga, S. Evidence of Mixed-Ligand Complexes in Cu-CHA by Reaction of Cu Nitrates with NO/NH_3 at Low Temperature. *ChemCatChem* **2019**, *11*, 3828−3838.
(17) Paolucci, C.; Khurana, I.; Parekh, A. A.; Li, S.; Shih, A. J.; Li, H.; Di Iorio, J. R.; Albarracin-Caballero, J. D.; Yezerets, A.; Miller, J. T.; et al. Dynamic Multinuclear Sites Formed by Mobilized Copper Ions in NO_x Selective Catalytic Reduction. *Science* **2017**, *357*, 898−903.
(18) Chen, L.; Janssens, T. V. W.; Vennestrøm, P. N.; Jansson, J.; Skoglundh, M.; Grönbeck, H. A Complete Multisite Reaction Mechanism for Low-Temperature NH_3-SCR over Cu-CHA. *ACS Catal.* **2020**, *10*, 5646−5656.
(19) Paolucci, C.; Parekh, A. A.; Khurana, I.; Di Iorio, J. R.; Li, H.; Albarracin Caballero, J. D.; Shih, A. J.; Anggara, T.; Delgass, W. N.; Miller, J. T.; et al. Catalysis in a Cage: Condition-Dependent Speciation and Dynamics of Exchanged Cu Cations in SSZ-13 Zeolites. *J. Am. Chem. Soc.* **2016**, *138*, 6028−6048.
(20) Paolucci, C.; Di Iorio, J. R.; Schneider, W. F.; Gounder, R. Solvation and Mobilization of Copper Active Sites in Zeolites by Ammonia: Consequences for the Catalytic Reduction of Nitrogen Oxides. *Acc. Chem. Res.* **2020**, *53*, 1881−1892.
(21) Chen, L.; Falsig, H.; Janssens, T. V. W.; Grönbeck, H. Activation of Oxygen on $(NH_3{-}Cu{-}NH_3)^+$ in NH_3-SCR over Cu-CHA. *J. Catal.* **2018**, *358*, 179−186.
(22) Negri, C.; Selleri, T.; Borfecchia, E.; Martini, A.; Lomachenko, K. A.; Janssens, T. V. W.; Cutini, M.; Bordiga, S.; Berlier, G. Structure and Reactivity of Oxygen-Bridged Diamino Dicopper(II) Complexes in Cu-Ion-Exchanged Chabazite Catalyst for NH_3-Mediated Selective Catalytic Reduction. *J. Am. Chem. Soc.* **2020**, *142*, 15884−15896.
(23) Oda, A.; et al. Spectroscopic Evidence of Efficient Generation of Dicopper Intermediate in Selective Catalytic Reduction of NO over Cu-Ion-Exchanged Zeolites. *ACS Catal.* **2020**, 12333−12339.
(24) Wang, X.; Chen, L.; Vennestrøm, P. N.; Janssens, T. V.; Jansson, J.; Grönbeck, H.; Skoglundh, M. Direct Measurement of Enthalpy and Entropy Changes in NH_3 Promoted O_2 Activation over Cu-CHA at Low Temperature. *ChemCatChem* **2021**, *13*, 2577−2582.
(25) Solomon, E. I.; Heppner, D. E.; Johnston, E. M.; Ginsbach, J. W.; Cirera, J.; Qayyum, M.; Kieber-Emmons, M. T.; Kjaergaard, C. H.; Hadt, R. G.; Tian, L. Copper Active Sites in Biology. *Chem. Rev.* **2014**, *114*, 3659−3853.
(26) DuBois, J. L.; Mukherjee, P.; Stack, T. D.; Hedman, B.; Solomon, E. I.; Hodgson, K. O. A Systematic K-edge X-ray Absorption Spectroscopic Study of Cu(III) Sites. *J. Am. Chem. Soc.* **2000**, *122*, 5775−5787.
(27) Gramigni, F.; Nasello, N. D.; Usberti, N.; Iacobone, U.; Selleri, T.; Hu, W.; Liu, S.; Gao, X.; Nova, I.; Tronconi, E. Transient Kinetic Analysis of Low-Temperature NH_3-SCR over Cu-CHA Catalysts Reveals a Quadratic Dependence of Cu Reduction Rates on Cu^{II}. *ACS Catal.* **2021**, *11*, 4821−4831.
(28) De-La-Torre, U.; Pereda-Ayo, B.; Gutiérrez-Ortiz, M. A.; González-Marcos, J. A.; González-Velasco, J. R. Steady-State NH_3-SCR Global Model and Kinetic Parameter Estimation for NO_x Removal in Diesel Engine Exhaust Aftertreatment with Cu/Chabazite. *Catal. Today* **2017**, *296*, 95−104.
(29) Bendrich, M.; Scheuer, A.; Hayes, R. E.; Votsmeier, M. Unified Mechanistic Model for Standard SCR, Fast SCR, and NO_2 SCR over a Copper Chabazite Catalyst. *Appl. Catal., B* **2018**, *222*, 76−87.
(30) Oka, K.; Ohori, T.; Itagaki, Y.; Osumi, K.; Ishikawa, N.; Dobashi, Y.; Wako, E. In *Improvement in Selective Catalytic Reduction Model Accuracy for Predicting NO_x Conversion at High Temperature*, SAE Technical Paper Series, 2018; pp 1−12.
(31) Eijima, W.; Shibata, G.; Shibayama, N.; Kobashi, Y.; Ogawa, H.; Shimizu, K.-i. Kinetic Modeling of Steady-State NH_3-SCR over a Monolithic Cu-CHA Catalyst. *Catal. Today* **2020**, *352*, 237−242.
(32) Kresse, G.; Hafner, J. Ab Initio Molecular Dynamics for Open-Shell Transition Metals. *Phys. Rev. B: Condens. Matter Mater. Phys.* **1993**, *48*, 13115−13118.
(33) Kresse, G.; Hafner, J. Ab Initio Molecular-Dynamics Simulation of the Liquid-Metalamorphous-Semiconductor Transition in Germanium. *Phys. Rev. B: Condens. Matter Mater. Phys.* **1994**, *49*, 14251−14269.
(34) Kresse, G.; Furthmüller, J. Efficient Iterative Schemes for Ab Initio Total-Energy Calculations Using a Plane-Wave Basis Set. *Phys. Rev. B: Condens. Matter Mater. Phys.* **1996**, *54*, 11169−11186.
(35) Kresse, G.; Furthmüller, J. Efficiency of Ab-Initio Total Energy Calculations for Metals and Semiconductors using a Plane-Wave Basis Set. *Comput. Mater. Sci.* **1996**, *6*, 15−50.
(36) Blöchl, P. E. Projector Augmented-Wave Method. *Phys. Rev. B: Condens. Matter Mater. Phys.* **1994**, *50*, 17953−17979.
(37) Kresse, G.; Joubert, D. From Ultrasoft Pseudopotentials to the Projector Augmented-Wave Method. *Phys. Rev. B: Condens. Matter Mater. Phys.* **1999**, *59*, 1758−1775.
(38) Perdew, J. P.; Burke, K.; Ernzerhof, M. Generalized Gradient Approximation Made Simple. *Phys. Rev. Lett.* **1996**, *77*, 3865−3868.
(39) Isseroff, L. Y.; Carter, E. A. Importance of Reference Hamiltonians Containing Exact Exchange for Accurate One-Shot GW Calculations of Cu_2O. *Phys. Rev. B: Condens. Matter Mater. Phys.* **2012**, *85*, No. 235142.
(40) Chen, L.; Janssens, T. V.; Grönbeck, H. A Comparative Test of Different Density Functionals for Calculations of NH_3-SCR over Cu-Chabazite. *Phys. Chem. Chem. Phys.* **2019**, *21*, 10923−10930.
(41) Grimme, S.; Antony, J.; Ehrlich, S.; Krieg, H. A Consistent and Accurate Ab Initio Parametrization of Density Functional Dispersion Correction (DFT-D) for the 94 Elements H-Pu. *J. Chem. Phys.* **2010**, *132*, No. 154104.
(42) Grimme, S.; Ehrlich, S.; Goerigk, L. Effect of the Damping Function in Dispersion Corrected Density Functional Theory. *J. Comput. Chem.* **2011**, *32*, 1456−1465.
(43) Mills, G.; Jónsson, H.; Schenter, G. K. Reversible Work Transition State Theory: Application to Dissociative Adsorption of Hydrogen. *Surf. Sci.* **1995**, *324*, 305−337.
(44) Henkelman, G.; Jónsson, H. Improved Tangent Estimate in the Nudged Elastic Band Method for Finding Minimum Energy Paths and Saddle Points. *J. Chem. Phys.* **2000**, *113*, 9978−9985.
(45) Nosé, S. A Unified Formulation of the Constant Temperature Molecular Dynamics Methods. *J. Chem. Phys.* **1984**, *81*, 511−519.
(46) Hoover, W. G. Canonical Dynamics: Equilibrium Phase-Space Distributions. *Phys. Rev. A* **1985**, *31*, 1695−1697.
(47) Gao, F.; Washton, N.; Wang, Y.; Kollár, M.; Szanyi, J.; Peden, C. Effects of Si/Al Ratio on Cu/SSZ-13 NH_3-SCR Catalysts: Implications for the Active Cu Species and the Roles of Brønsted Acidity. *J. Catal.* **2015**, *331*, 25−38.
(48) Chorkendorff, I.; Niemantsverdriet, J. W. *Concepts of Modern Catalysis and Kinetics*; John Wiley & Sons, 2017; pp 107−112.

https://doi.org/10.1021/acscatal.1c03973
ACS Catal. 2021, 11, 14395−14407

(49) Piccini, G.; Alessio, M.; Sauer, J. Ab Initio Calculation of Rate Constants for Molecule-Surface Reactions with Chemical Accuracy. *Angew. Chem., Int. Ed.* **2016**, *55*, 5235−5237.
(50) Jørgensen, M.; Chen, L.; Grönbeck, H. Monte Carlo Potential Energy Sampling for Molecular Entropy in Zeolites. *J. Phys. Chem. C* **2018**, *122*, 20351−20357.
(51) Chen, L.; Jansson, J.; Skoglundh, M.; Grönbeck, H. Mechanism for Solid-State Ion Exchange of Cu+ into Zeolites. *J. Phys. Chem. C* **2016**, *120*, 29182−29189.
(52) Chen, L.; Falsig, H.; Janssens, T. V. W.; Jansson, J.; Skoglundh, M.; Grönbeck, H. Effect of Al-distribution on oxygen activation over Cu−CHA. *Catal. Sci. Technol.* **2018**, *8*, 2131−2136.
(53) Li, J.; Li, S. New Insight into Selective Catalytic Reduction of Nitrogen Oxides by Ammonia over H-form Zeolites: A Theoretical Study. *Phys. Chem. Chem. Phys.* **2007**, *9*, 3304−3311.
(54) Borfecchia, E.; Negri, C.; Lomachenko, K. A.; Lamberti, C.; Janssens, T. V. W.; Berlier, G. Temperature-Dependent Dynamics of NH_3-Derived Cu Species in the Cu-CHA SCR Catalyst. *React. Chem. Eng.* **2019**, *4*, 1067−1080.
(55) Akter, N.; Chen, X.; Parise, J.; Boscoboinik, J. A.; Kim, T. Effects of Copper Loading on NH_3-SCR and NO Oxidation over Cu Impregnated CHA Zeolite. *Korean J. Chem. Eng.* **2018**, *35*, 89−98.
(56) Fahami, A. R.; Günter, T.; Doronkin, D. E.; Casapu, M.; Zengel, D.; Vuong, T. H.; Simon, M.; Breher, F.; Kucherov, A. V.; Brückner, A.; et al. The Dynamic Nature of Cu Sites in Cu-SSZ-13 and the Origin of the Seagull NO_x Conversion Profile during NH_3-SCR. *React. Chem. Eng.* **2019**, *4*, 1000−1018.
(57) Jones, C. B.; Khurana, I.; Krishna, S. H.; Shih, A. J.; Delgass, W. N.; Miller, J. T.; Ribeiro, F. H.; Schneider, W. F.; Gounder, R. Effects of Dioxygen Pressure on Rates of NO_x Selective Catalytic Reduction with NH_3 on Cu-CHA Zeolites. *J. Catal.* **2020**, *389*, 140−149.
(58) Campbell, C. T. Future Directions and Industrial Perspectives Micro- and Macro-Kinetics: Their Relationship in Heterogeneous Catalysis. *Top. Catal.* **1994**, *1*, 353−366.

https://doi.org/10.1021/acscatal.1c03973
ACS Catal. 2021, 11, 14395−14407